

Effect of Hydrogen on Flaking of Carbon Films on Mo and W

K. Heinola^{1,*}, T. Ahlgren¹, W. Rydman¹, J. Likonen², L. Khriachtchev³, J. Keinonen¹ and C. H. Wu⁴

¹ Accelerator Laboratory, P.O. Box 64, FIN-00014 University of Helsinki, Finland

² VTT Processes, P.O. Box 1608, FIN-02044 VTT, Finland

³ Laboratory of Physical Chemistry, P.O. Box 55, FIN-00014 University of Helsinki, Finland

⁴ MPI für Plasmaphysik, Boltzmannstrasse 2, D-85748 Garching bei München, Germany

Received June 26, 2003; accepted August 11, 2003

PACS Ref: 68.35.Gy

Abstract

Flaking of carbon film was studied by depositing hydrogen doped carbon films on tungsten and molybdenum substrates. Topographies of the carbon coatings were analyzed with scanning electron microscopy and three-dimension profilometer. Secondary ion mass spectrometry and Raman spectra analysis was used to determine the hydrogen concentration and the number of sp^3 bonds in the films, respectively. Carbon film properties varied from tetrahedral amorphous carbon (ta-C) to hard hydrogenated amorphous carbon (a-C:H). Carbon coatings hold large residual stresses, which are released during or after deposition. Typical stress relief patterns were observed. In most samples buckling started at some dislocation or at the edge of the film and adhesion energy was deduced from the sizes of the stress relief patterns. It was observed, that carbon films were more adherent to tungsten than to molybdenum and that codeposited hydrogen had a significant effect to flaking propagation in the carbon films.

1. Introduction

Carbon, tungsten and molybdenum are good candidates for plasma facing wall and divertor material in the next step fusion reactor. So far, carbon and tungsten have been chosen to be used in ITER, where materials must withstand high temperatures as well as physical and chemical sputtering [1]. Surface of the material plays a key role in the recycling of hydrogen fuel and particles sputtered from the plasma facing material cause radiative power losses to the plasma. Macroscopic amounts of the material can be lost from the surface as flakes. Especially carbon flakes can contain large amounts tritium ([2] and references therein). Flake formation has to be low in order to minimise the centimetre scale erosion of wall material and the total amount of hazardous tritium in the fusion device.

Carbon is used in divertor region with extreme temperature loads, i.e., strike-points, because of its good thermal fatigue resistance. Carbon sublimates instead of melting, but its chemical erosion due to hydrogen is high. Molybdenum and tungsten have good thermal conductivities, low physical sputtering yields and no chemical sputtering due to hydrogen, thus they are good candidates as plasma facing material in other divertor regions, i.e., side wall and dome.

Eroded carbon particles redeposit on other regions of the wall and divertor surface. Redeposition depends on the sticking of the hydrocarbons to the substrate or target surface, where they form rigid diamond-like carbon (DLC) films, which hold large compressive stresses. In thin films the formation of these residual stresses depend mainly on

deposition energy, codeposited hydrogen and substrate temperature. The compressive stresses produce buckling of the films. In buckled area the film is lifted up from substrate and film adhesion finds its minimum. Buckling is coupled with film/substrate interface cracking. Buckling-driven film delamination grows along a certain front [3]. Growing of the delamination can lead to peeling and cracking of the film. To model this, hydrogen doped carbon films were deposited on tungsten and molybdenum substrate. Flaking of carbon films was studied using different deposition temperatures, film thicknesses and hydrogen concentrations.

2. Experimental

The samples studied were prepared by DIARC-Technology Inc. using the DIARC method [4]. Several different sets of carbon film samples were grown. Carbon films were deposited on tungsten and molybdenum substrates, which in turn were earlier grown on monocrystalline Si. The W–Si and Mo–Si combinations form a hard compound so the tungsten and molybdenum layers form a substrate [5]. Carbon film thicknesses were about 250 and 500 nm on both substrate types. In addition, there were about 750, 1000 and 1250 nm films deposited on molybdenum substrate. Deposition temperatures were room temperature, 100 and 300 °C. Samples were grown in vacuum (H free) and in methane atmosphere (films containing hydrogen). CH_4 deposition pressures used were 10^{-4} and 10^{-3} mbar. The thick 750–1250 nm films were deposited in vacuum at RT and 100 °C. The aim was to understand the effect of hydrogen to the deposition of carbon films with different thicknesses and temperatures.

Secondary ion mass spectrometry (SIMS) and Raman spectroscopy[21,22] were used to determine the hydrogen concentrations and carbon sp^3/sp^2 bonding ratio in the films, respectively. 1H concentrations were measured using 5 keV O_2^+ primary ions. Primary ion current was 400 nA and analyzed area $320 \times 460 \mu m^2$. The SIMS instrument was calibrated for hydrogen with a 27 keV and $1.6 mC/cm^2$ 1H implanted DLC foil. Depositing carbon films in CH_4 atmosphere produced relatively constant hydrogen concentrations throughout the films. With depositing pressure 10^{-4} mbar hydrogen concentrations were 1.6–2.0 at.% in different samples. Higher depositing pressure 10^{-3} mbar resulted to higher hydrogen concentration of about 6 at.%. Scanning electron microscopy SEM (Zeiss DSM 692) and 3D stylus profilometer (KLA-Tencor

* e-mail: kalle.heinola@helsinki.fi

P-15 Profiler) were used in analyzing the topographies of the samples and the dimensions of the different stress relief patterns. The radius of the stylus was 2 μm , scan speed 50 $\mu\text{m/s}$, applied force 2 mg and sampling rate 50 Hz.

3. Results and discussion

3.1. Film growth

Lifshitz [6] proposed that carbon film growth process goes via shallow subsurface implantation, i.e., subplantation. In the subplantation model, carbon ions with energies above a certain threshold energy penetrate the surface into subsurface layers increasing the local carbon density. Carbon ions with lower energies will be implanted closer to the surface. They remain at their lowest energy state and form sp^2 hybridised bonds. Carbon ions in subsurface high density area form bulk-carbon phase and become sp^3 hybridised. At higher carbon ion energies the excess density decreases to zero via thermalisation and relaxation processes of the dense region. During the carbon film growth, part of the carbon ions densify the subsurface and form sp^3 's while the rest end up to the surface giving the film growth.

Although the growth mechanism of a-C:H film is a much more complicated process [7], the behaviour of implanted ions can be individually approached via subplantation. H prefers bonding with carbon sp^3 's. As a result a large part of the sp^3 bonds can be saturated due to hydrogen. a-C:H films with high hydrogen concentration and high sp^3 ratio have low density and are therefore called soft a-C:H films. Films with higher density have less hydrogen and lower sp^3 ratio and are categorized as hard a-C:H films. Films which have none or low hydrogen concentration but high sp^3 content and high densities, are called ta-C or ta-C:H films, respectively. In this work, films grown at RT in vacuum or in CH_4 deposition pressure 10^{-4} mbar had sp^3 's between 50–70%. Films deposited at 300 $^\circ\text{C}$ hold sp^3 's from 0 to 35% increasing with the hydrogen concentration. Diamond bonds sp^3 convert into graphite bonds sp^2 at temperatures over 350 $^\circ\text{C}$, so the latter films can be graded as a-C:H. In turn, the former films with high sp^3 and low or none hydrogen concentration can be thought as ta-C or ta-C:H. Nevertheless, it is worth mentioning that a complete film categorisation should also include film density measurements.

3.2. Stress relief patterns

Ion bombardment deposition generates compressive stresses in the film [8]. Ions penetrate directly into the subsurface region or indirectly by knock-on processes. In densified region the strain energy of the film is increased, which tends to move the implanted ions to energetically favoured direction, i.e., the surface. Implanted atoms are however immobile because of the repulsive forces of the surrounding atoms. This builds up stress inside the film which can be relaxed via thermal spikes generated by bombarding ions. Relaxed atoms diffuse back to the surface to the lower sp^2 density. Incorporated sp^2 bonds in the film tend to produce compressive stresses, because their specific volume is $1.5\times$ that of sp^3 bonds [9]. The

film's residual stress consists of thermal and deposition, i.e., intrinsic, components

$$\sigma_{\text{res}} = \sigma_{\text{therm}} + \sigma_{\text{intr.}}$$

Thermal stress arises simply from the differences of thermal expansion coefficients of the film and the substrate and is well understood. Intrinsic stress is a more complicated component and depends on, e.g., deposition conditions, film thickness, thermal spikes, volume changes inside the film, oxidation of the film surface and film structure in general as mentioned above. The nature of intrinsic stress can vary from compressive to tensile in line with different deposition parameters in different materials. Although intrinsic stress is usually the dominant stress component, a final explanation for its origin in different films and materials is still lacking.

Stress relaxation takes place during or after deposition, which can be seen in different forms of stress relief patterns. In this work it was not determined whether flaking started in the deposition chamber or in room atmosphere. Several reports on formation of DLC film stress relief patterns can be found in the literature [10–13]. Similar relief patterns on metallic and other hard coating materials have been reported [14–16]. Stress relief patterns can evolve with time [16]. Exposing films to surrounding atmosphere can boost or even initiate formation of patterns [17], where the film debonding can begin by nucleation and growth of a gas bubble at the film/substrate interface [18].

In this work, following stress relief behaviour was observed: (a) In most cases film buckling started at some defect in the film or from the edge of the film proceeding to the centre. (b) Different stress relief patterns were detected: cracking of the film, straight-sided patterns with and without cracks on ridges (Fig. 1), sinusoidal patterns (Figs. 1, 3 and 4), string-of-beads patterns (Fig. 1), peeling by layers (Fig. 5). (c) Patterns propagated in random directions branching and connecting with other patterns. Buckling propagated with constant physical dimension, but increasing with film thickness. (d) Film adhesion to

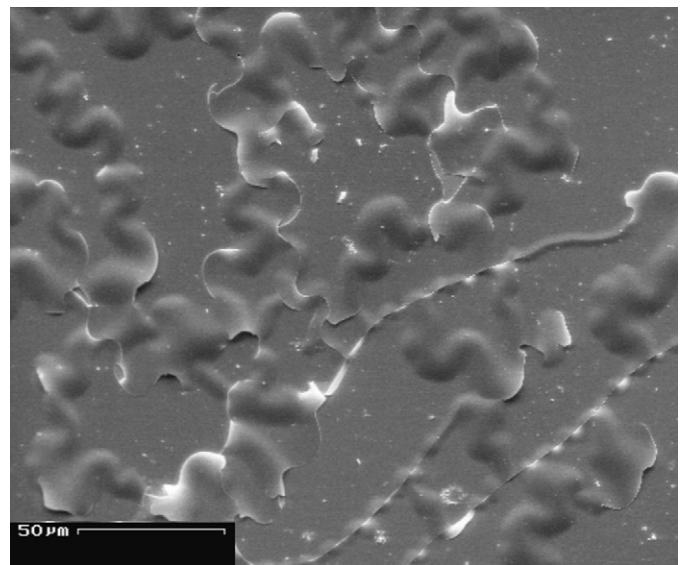


Fig. 1. Sinusoidal, straight-sided and string of beads stress-relief patterns on 250 nm carbon film seen with SEM. Film was deposited on molybdenum at RT in CH_4 pressure of 10^{-4} mbar.

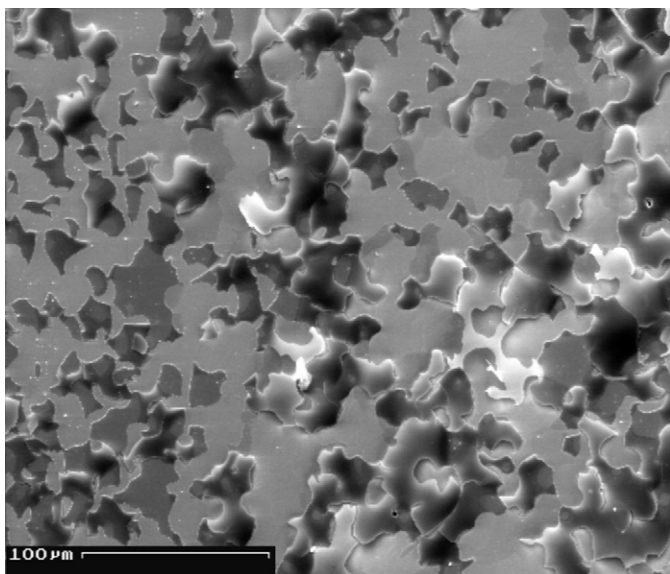


Fig. 2. Higher CH_4 pressure (10^{-3} mbar) generated flaking of carbon film on molybdenum seen with SEM. Other deposition parameters similar as in Fig. 1.

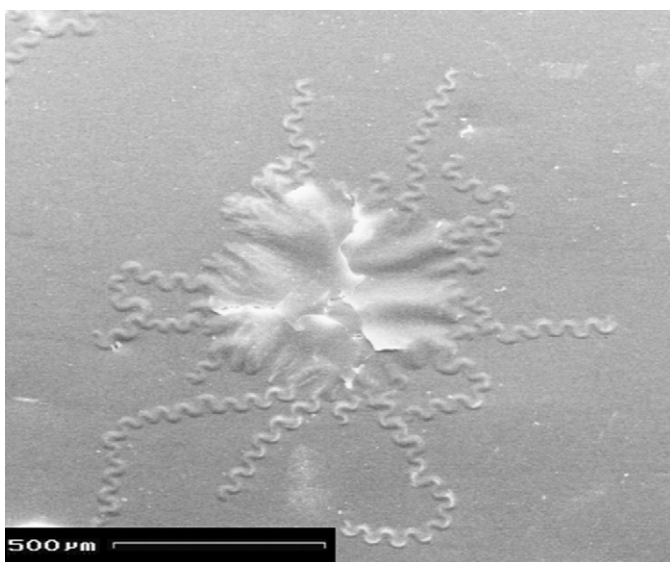


Fig. 3. SEM picture of sinusoidal patterns starting at dislocation in the film with thickness 250 nm and molybdenum as substrate. Codeposited hydrogen (CH_4 pressure of 10^{-4} mbar) enhanced adhesion at 300°C .

molybdenum was clearly poorer than to tungsten. Nearly all of the patterns were observed on molybdenum. This was presumably due to oxidation of the molybdenum substrates as they were kept in room atmosphere for a few weeks before carbon deposition. (e) In vacuum at deposition temperature 300°C , over 50% of the film had flaked off independent of the substrate type. Deposition in CH_4 pressure enhanced film adhesion at high temperature. (f) At RT and 100°C deposition in CH_4 pressure worsened adhesion to the substrate. (see Figs. 2 and 6.) (g) Increasing film thickness had a decreasing effect to the adhesion. At film thickness over 1000 nm an increase in the deposition temperature improved adhesion to the substrate.

From these studies it is evident that the intrinsic stress is increasing with film thickness. The width, height and wavelength of sinusoidal patterns grow when thickness

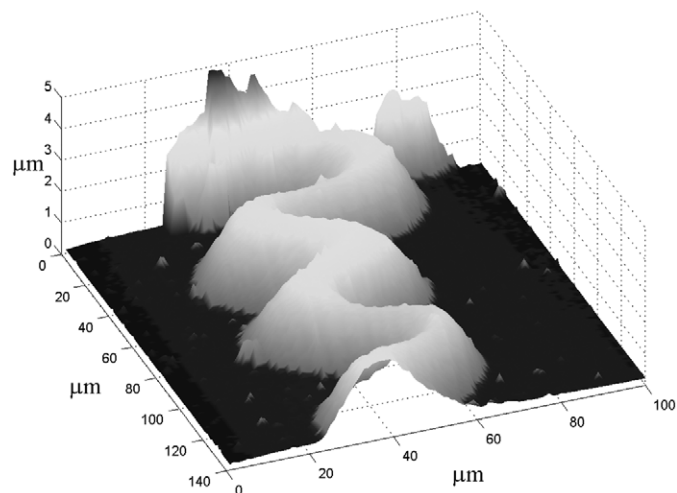


Fig. 4. 3D profilometer picture of sinusoidal pattern from Fig. 3.

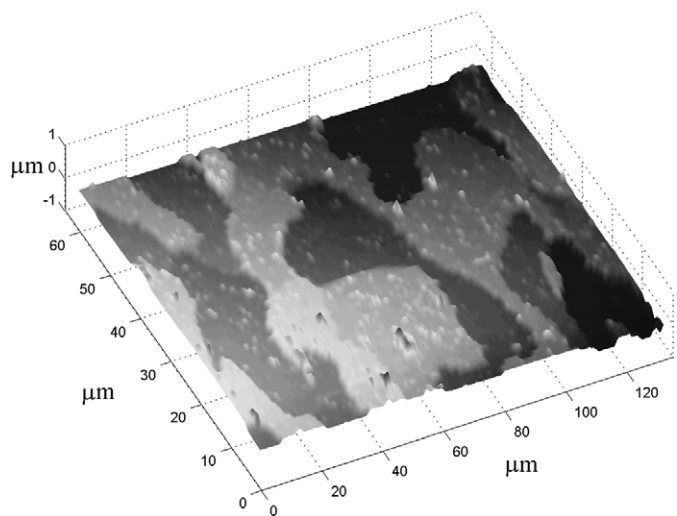


Fig. 5. Peeling by layers at 500 nm carbon film. molybdenum substrate visible (dark shaded areas on the right). Film was deposited at RT in CH_4 pressure of 10^{-3} mbar.

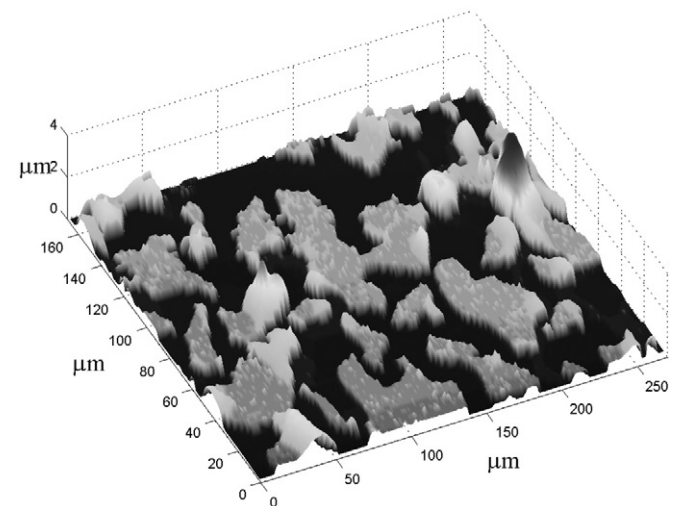


Fig. 6. C film flaked off leaving sharp-edged carbon film islands on molybdenum substrate (dark areas). Deposition was done at 100°C , other parameters similar as in Fig. 5.

increases. Deposition temperature had an obvious effect to the film adhesion. At 300°C , which is near graphitisation temperature, the major part of the film was delaminated from the substrate. These films, with no sp^3 bonds, were

Table I. Calculated U_a values for samples with wrinkles. See text for details.

Substrate	thickness (nm)	T_{dep} (°C)	CH ₄ press. (mbar)	l (μm)	w_0 (μm)	U_a (J/m ²)
1. Mo	170	RT	10 ⁻⁴	9	0.7	0.42
2. Mo	380	300	10 ⁻⁴	33	2.3	0.28
3. Mo	490	100	10 ⁻⁴	41	3.2	0.49

brittle with low adhesion. Films deposited at RT and 100 °C were more adherent. Besides graphitization also differences in the linear expansion coefficients between the film and substrate can produce stress into the film, which enhances cracking of the film.

The contribution of hydrogen concentration to the residual stress was apparent, but needs more detailed discussion. With the thinnest 250 nm films deposited at RT, the increase in CH₄ deposition pressure increased flaking of the film markedly (Figs. 1 and 3). At 100 °C the effect was same, but not so strongly evident. Here the increase in film thickness started delamination process again. At deposition temperature 300 °C the effect of hydrogen was the opposite. At this temperature, the rupture of the vacuum deposited films was as mentioned above, but in contrast with films deposited at lower temperatures (RT and 100 °C), these were less detached with increasing CH₄ deposition pressure. Also the ratio of sp³ bondings increased with CH₄ pressure, still remaining fairly low compared with the low-temperature films. As a result, the deposition temperature together with film thickness and the amount of codeposited hydrogen can be considered as competitive effects in the formation of residual stress in thin films, even though the latter is more dominant.

3.3. Comparison with theory

Thin film buckling phenomena can be examined with a general theory of plates [10]. The film is considered as a thin plate, which is adhered to the substrate. The plate is under biaxial stresses, which causes bending of the plate [19,20]. The plate behaviour under stress can be modelled with Föppl–von Karman (FvK) equations, which consist of two fourth-order, second-degree, partial differential equations. A buckling equation can be obtained from the FvK equations using expressions from the linear theory [20]

$$D \left(\frac{\partial w^4}{\partial x^4} + 2 \frac{\partial w^4}{\partial x^2 \partial y^2} + \frac{\partial w^4}{\partial y^4} \right) + \sigma_x h \frac{\partial w^2}{\partial x^2} + \sigma_y h \frac{\partial w^2}{\partial y^2} + 2\tau_{xy} h \frac{\partial w^2}{\partial x \partial y} + f = 0, \quad (1)$$

where D is flexural rigidity of the film, h film thickness, x and y coordinates relative to the substrate and w film deflection defined in elastic theory, σ and τ are compressive stress and shear stress, f is any external force.

Nir [10] discussed different solutions to Eq. (1). Matuda *et al.* [11] used an approximate cross-sectional shape of a sinusoidal wrinkle

$$w(x) = \frac{w_0}{2} \left(1 + \cos \frac{2\pi x}{l} \right) \quad (2)$$

to derive an expression for the adhesion energy per unit length

$$U_a = \frac{\pi^4 (w_0/l)^2 E h^3}{12(1-\nu^2)} \frac{L}{l^2(L-l)}, \quad (3)$$

where w_0 is the maximum height of the dislocation, l its width, h film thickness, E and ν Young modulus and Poisson ratio, respectively. U_a is adhesion energy per unit length for two orthogonal wrinkles of width l extending in the x and y direction over a square of width L . Table I shows calculated adhesion energy values for samples with sinusoidal patterns as dominant stress relief pattern. Sample 3 was included as a reference with smooth surface, but having only one clear sinusoidal pattern branching from a dislocation into three similar patterns. Estimated adhesion energy values are of the same order as in [11,13], despite the fact that in [11] the carbon films were grown on glass substrates.

4. Conclusions

H doped carbon films were deposited on tungsten and molybdenum substrates. Different deposition parameters were used in order to generate flaking of the films. In general, carbon films observed had good adhesion, but film delamination occurred in some samples. Various stress relief patterns were seen. Stress-relief patterns were used to estimate adhesion energy of the films. Flaking was strongly dependent on the hydrogen concentration in the film. At low deposition temperatures film adhesion decreased with increasing hydrogen concentration. On the contrary, at 300 °C increasing hydrogen concentration decreased film flaking. The dynamic effect of codeposited hydrogen stands for a competing behaviour of the residual stress evolution. At high deposition temperatures the differences in linear expansion coefficients of the film and the substrate can play a dominant role. Codeposited hydrogen decreases this effect by forming the film into soft a-C:H. This was seen in the increase of sp³ ratio and adhesion to the substrate.

Acknowledgment

We thank the Electron Microscopy Unit of the Institute of Biotechnology—University of Helsinki for providing laboratory facilities. J. Kolehmainen and S. Tervakangas (DIARC-Technology Inc.) are gratefully acknowledged for the sample preparation. Research was supported by EURATOM and the Finnish National Technology Agency (TEKES).

References

1. Federici, G. *et al.*, Nucl. Fusion **41**, 1967 (2001).
2. Penzhorn, G. *et al.*, Fusion Eng. Des. **56–57**, 105 (2001).
3. Jensen, H. M. and Sheinman, I., Int. J. Solids Struct. **39**, 3373 (2002).
4. Vainonen, E. *et al.*, J. Appl. Phys. **82**, 3791 (1997).
5. Kolehmainen, J., DIARC-Technology Inc., Helsinki, Finland, private communication.

6. Lifshitz, Y., Kasi, S. R., Rabalais, J. W. and Eckstein, W., *Phys. Rev. B* **41**, 10648 (1990).
7. von Keudell, A., Meier, M. and Hopf, C., *Diam. Relat. Mater.* **11**, 969 (2002).
8. Davis, C. A., *Thin Solid Films* **226**, 30 (1993).
9. Clyne, T. W., "Encyclopedia of Materials: Science and Technology," vol. I (Eds. K. H. J. Buschow *et al.*) (Elsevier, Oxford, 2001).
10. Nir, D., *Thin Solid Films* **112**, 41 (1984).
11. Matuda, N., Baba, S. and Kinbara, A., *Thin Solid Films* **81**, 301 (1981).
12. Gille, G. and Rau, B., *Thin Solid Films* **120**, 109 (1984).
13. Iyer, B. S., Harshavardhan, S. K. and Kumar, V., *Thin Solid Films* **256**, 94 (1995).
14. Chopra, K. L., "Thin Film Phenomena," (McGraw-Hill, New York, 1969).
15. Meyer, D. C., Klingner, A., Holz, Th. and Paufler, P., *Appl. Phys.* **A69**, 657 (1999).
16. Ogawa, K., Ohkoshi, T., Takeuchi, T., Mizoguchi, T. and Masumoto, T., *Jpn. J. Appl. Phys.* **25**(5) 695 (1986).
17. Kinbara, A., Baba, S., Matuda, N. and Takamisawa, K., *Thin Solid Films* **84**, 205 (1981).
18. Peng, X. L. and Clyne, T. W., *Thin Solid Films* **312**, 219 (1998).
19. Landau, L. D. and Lifshitz, E. M., "Theory of Elasticity," (Pergamon Press, New York 1959).
20. Timoshenko, S. and Woinowsky-Krieger, S., "Theory of Plates and Shells," (McGraw-Hill, New York, 1959).
21. Stanishevsky, A. and Khriachtchev, L., *J. Appl. Phys.* **86**, 7052 (1999).
22. Khriachtchev, L., Vainonen-Ahlgren, E., Sajavaara, T., Ahlgren, T. and Keinonen, J., *J. Appl. Phys.* **88**, 2118 (2000).